Atmos. Chem. Phys. Discuss., 12, 24955–24984, 2012
www.atmos-chem-phys-discuss.net/12/24955/2012/
doi:10.5194/acpd-12-24955-2012

Atmospheric Chemistry and Physics Discussions

On the export of reactive nitrogen from Asia: NO_x partitioning and effects on ozone

T. H. Bertram[1,*], A. E. Perring[1,], P. J. Wooldridge[1], J. Dibb[3], M. A. Avery[4], and R. C. Cohen[1,2]**

[1]Department of Chemistry; University of California, Berkeley, USA
[2]Department of Earth and Planetary Science, University of California, Berkeley, USA
[3]Institute for the Study of Earth, Oceans, and Space, University of New Hampshire, USA
[4]NASA Langley Research Center; Hampton, VA, USA
[*]now at: Department of Chemistry and Biochemistry, University of California, San Diego, USA
[**]now at: NOAA Earth System Research Laboratory, Boulder, CO, USA

Received: 4 September 2012 – Accepted: 12 September 2012
– Published: 21 September 2012

Correspondence to: R. C. Cohen (rccohen@berkeley.edu)

Published by Copernicus Publications on behalf of the European Geosciences Union.

Abstract

The partitioning of reactive nitrogen (NO_y) was measured over the remote North Pacific during spring 2006. We use these observations to assess the impact of increasing emissions of nitrogen oxides in East Asia on ozone (O_3) production rates over the remote Pacific and the intercontinental transport of O_3 and its precursors to North America. Aircraft observations of speciated NO_y, made between 25° and 55° N, confirm a controlling role for peroxyacyl nitrates in NO_x production in aged Asian outflow, accounting for more than 60 % of NO_y above 5 km, while thermal dissociation limits their contribution to less than 10 % in the lower troposphere. The observations reveal the extreme sensitivity of the remote Pacific to future changes in NO_x loadings, with an experimentally determined crossover point between net O_x destruction and net O_x production of 60 pptv NO_x. Using simultaneous observations of speciated NO_y and wind speed, we calculate the flux of reactive nitrogen through the meridional plane of 150° W (between 25° and 55° N) to be 0.007 ± 0.002 Tg N day^{-1}, which provides an upper limit of 15 % on the export efficiency of NO_y from East Asia. Analysis of the subsiding plumes in the sampling domains suggests that episodic dry subsidence events play an important role in the intercontinental transport of ozone and its precursors from East Asia to North America.

1 Introduction

The partitioning of reactive nitrogen (NO_y), among the various oxides of nitrogen (e.g. nitric oxide (NO), nitrogen dioxide (NO_2), peroxyacyl nitrates (ΣPNs), alkyl and multifunctional nitrates (ΣANs), nitric acid (HNO_3) and others), determines the spatial scales by which NO_x ($NO_x \equiv NO + NO_2$), or its temporary reservoirs, are transported. As a result, NO_y partitioning impacts the spatial distribution of nitrogen deposition and the production rates of both ozone (O_3) and secondary organic and inorganic aerosol on local, regional and global scales.

Determining the magnitude and distribution of the NO_x oxidation products, which can act as either temporary or permanent NO_x reservoirs, is critical for understanding the global distribution of NO_x in the troposphere and its subsequent effects on O_3. NO_x is removed from the catalytic ozone production cycle following the three-body reaction of NO_2 with the hydroxyl radical to produce HNO_3, as shown in Eq. (1). NO_2 can also react directly with peroxy radicals to form a peroxy nitrate (RO_2NO_2, Eq. 2), the most abundant being peroxy acetyl nitrate (or PAN) a derivative of acetaldehyde (Singh et al., 1985, 1986). Further, the NO_x cycle can be terminated through the formation of alkyl or multifunctional nitrates ($RONO_2$) following the reaction of NO with RO_2 (Eq. 3) (Calvert and Madronich, 1987; Trainer et al., 1991).

$$NO_2 + OH + M \rightarrow HNO_3 + M \quad (1)$$

$$NO_2 + RO_2 + M \leftrightarrow RO_2NO_2 + M \quad (2)$$

$$NO + RO_2 + M \rightarrow RONO_2 + M \quad (3)$$

NO_2 also reacts directly with O_3, producing the nitrate radical (NO_3), which quickly reaches thermodynamic equilibrium with dinitrogen pentoxide (N_2O_5) (Eqs. 4–5) (Noxon et al., 1978; Platt et al., 1980). This loss process occurs primarily at night due to the strong visible light absorption and subsequent dissociation of NO_3 as well as rapid reaction with NO (which is significantly reduced at night). Together these reactions limit the steady-state lifetime of NO_3 to seconds in daytime.

$$NO_2 + O_3 \rightarrow NO_3 + O_2 \quad (4)$$

$$NO_2 + NO_3 + M \leftrightarrow N_2O_5 + M \quad (5)$$

Additionally, nitrous acid (HONO), formed through the hydrolysis of NO_2 has been shown to be a significant component of NO_y at night near the surface (Finlayson-Pitts et al., 2003). The partitioning of reactive nitrogen between the various NO_x oxidation products is of great importance as each reservoir (e.g. RO_2NO_2, $RONO_2$, HNO_3 and N_2O_5) has a drastically different lifetime in the atmosphere. ΣPNs are largely insoluble (e.g. the Henry's Law Constant for PAN is 2–5 $M\,atm^{-1}$ at 273 °K) (Sander, 1999),

have low accommodation coefficients (γ = 0.0001) for heterogeneous uptake (Kirchner et al., 1990), and measurements have shown them to have small deposition velocities relative to other constituents of NO_y (Farmer et al., 2006; Turnipseed et al., 2006; Wolfe et al., 2009) leading to longer atmospheric lifetimes. However, ΣPNs are thermally unstable at warm temperatures and will act as a net source of NO_x in warm climates (Lamarque et al., 1996; Moxim et al., 1996; Horowitz and Jacob, 1999; Heald et al., 2003; Hudman et al., 2004). The PAN lifetime against thermal decomposition increases from hours to days in the BL to months in the UT where lower temperatures drive the equilibrium shown in Eq. (2) to the right, toward RO_2NO_2 (Talukdar et al., 1995). Nitric acid is largely soluble (e.g. the Henry's Law Constant for HNO_3 is 2–8 × 10^5 $M\,atm^{-1}$ at 273 °K) (Sander, 1999), and has a significant accommodation coefficient for heterogeneous removal (Choi and Leu, 1998; Arora et al., 1999; Tolocka et al., 2002) and a large deposition velocity (Munger et al., 1996, 1998). As a result, production of HNO_3 is viewed as an irreversible sink for NO_x. Alkyl nitrates (ΣANs) are removed following reaction with OH and O_3. In addition, hydroxyl- and multifunctional nitrates, which comprise a large fraction of ΣANs, especially in regions of strong biogenic influence (Day et al., 2003), are thought to be removed effectively via deposition and heterogeneous removal processes (Farmer et al., 2006). In the presence of high surface area loadings N_2O_5 can be hydrolyzed forming HNO_3 or $ClNO_2$ on chloride containing particles (Bertram and Thornton, 2009). These chemical lifetimes and the associated partitioning among different NO_y species determine the extent to which NO_x is present in the atmosphere far from its source and thus affect the rate of ozone production (e.g. Hudman, et al., 2004) and nitrogen deposition (e.g. Munger, et al., 1996), downwind of the source region.

NO_y in the free troposphere is thought to be composed primarily of PAN and HNO_3 (Li et al., 2004; Parrish et al., 2004b). This idea is based on the arguments that: (i) NO_x sources other than aircraft and lightning are confined to the boundary layer, (ii) the NO_x lifetime is significantly shorter than the time scale for transport to the free troposphere, and (iii) ΣANs are not particularly important (Buhr et al., 1990; Shepson et al., 1993).

The latter point has been challenged with direct observations of ΣANs in the planetary boundary layer and in the free troposphere (Day et al., 2003).

Observations show that NO_x emissions are rapidly increasing in the developing world (Richter et al., 2005). These increases are projected to be responsible for an increase in O_3 in the remote atmosphere, where O_3 production is largely NO_x limited (Fishman et al., 1979). However, a thorough understanding of the export efficiency and the subsequent processes governing the transport and chemical evolution of NO_y in the outflow from urban centers is essential to determining the extent to which the dramatic regional changes observed by Richter et al. (2005) are having a global impact. Recent analyses of aircraft observations have provided important tests of the amount of NO_y exported from continental sources and the mechanisms by which it is injected into the free troposphere (Heald et al., 2003; Hudman et al., 2004; Li et al., 2004; Parrish et al., 2004a). The most rapid NO_x increases are in Eastern China (e.g. Richter et al., 2005; Q. Zhang et al., 2007, 2009; L. Zhang et al., 2008; Walker et al., 2010), making the study of Asian outflow plumes of particular interest (Heald et al., 2003).

Observations of the partitioning of NO_y (between NO_x, ΣPNs, ΣANs, HNO_3 and other minor components) are limited in the free troposphere, particularly over the remote North Pacific. This is in part due to the difficulty of accessing the region and the requirement for multiple instruments to measure each individual component on a comparable sampling frequency. The free troposphere over the Pacific Ocean has been studied during multiple aircraft missions over the past 15 yr. However, these measurements were confined closely to either the Asian or North American Continents, with only a select number of transpacific flights that sampled the remote Pacific. The scientific objectives of earlier flight campaigns was the characterization of Asian outflow plumes near the source region (e.g. PEM West A, PEM West B and TRACE-P, Hoell et al., 1996, 1997; Jacob et al., 2003). Transit flights from the United States to the sampling region proved instructive in assessing the extent of transport and transformation of the Asian plumes (Heald et al., 2003). The Intercontinental Transport and Chemical Transformation 2002 (ITCT 2K2) Experiment made observations of Asian plumes transported to

North America during spring (Parrish et al., 2004a). Until the spring of 2006, the main transport corridor between Asia and North America was left largely unmeasured. In the following we describe observations of the partitioning of NO_y in Asian outflow over the remote Pacific using direct measurements of speciated NO_y (NO_x, ΣPNs, ΣANs and HNO_3) made between the surface and 12 km during the spring of 2006 and discuss the implications of these observations for our understanding of atmospheric chemistry over the Pacific.

2 Experimental methods

2.1 Intercontinental chemical transport experiment – phase B (INTEX-B)

We use observations obtained during the INTEX-B campaign, conducted out of Honolulu, HI and Anchorage, AK during April and May of 2006 using the NASA DC-8. Research flights were primarily conducted during daytime (88 % of the observations were made at SZA < 90°); the only nighttime flight was the transit between Honolulu and Anchorage. In the following analysis all observations were used. The principle objective of the INTEX-B campaign was to characterize the transport of Asian pollution, which is most frequent and rapid in spring, during periods of strong frontal activity (Yienger et al., 2000). Research flights were designed to sample pollution lofted from the Asian boundary layer (BL) by cold frontal activity and transported across the Pacific toward North America in the free troposphere. Observations highlighted in this study include in situ measurements of ozone, NO, NO_2, total peroxy nitrates (ΣPNs), total alkyl and multifunctional nitrates (ΣANs) and nitric acid (HNO_3) (Thornton et al., 2000; Day et al., 2002; Fairlie et al., 2007). Aircraft flight tracks are shown in Fig. 1a, where sampling legs north of 35° N are shown in black and sampling legs south of 35° N are shown in grey. The 35° N threshold was chosen as satellite observations and model analyses of enhancements in carbon monoxide, indicative of transpacific transport of Asian pollution, have shown strong influence north of 35° N (L. Zhang et al., 2008; Hsu et al.,

2012) coinciding with the westward movement of air above the Pacific High. The corresponding mean vertical profile in temperature for the two sampling regions is shown in Fig. 1b, highlighting an approximately 10 °C difference in temperature between the two regions from the surface through the mid troposphere. The implications of the observed temperature difference on the reactive nitrogen budget are discussed in detail in Sect. 3.2.

2.2 Thermal dissociation – laser induced fluorescence

Observations of NO_2, ΣPNs, ΣANs and HNO_3 were made using Thermal Dissociation – Laser Induced Fluorescence (TD-LIF) (Thornton et al., 2000; Day et al., 2002). Briefly, NO_2 fluorescence is detected following excitation of a specific jet-cooled rovibronic transition at 585 nm. The resulting fluorescence is collected by a PMT at 90° to the laser axis, which is both optically and temporally filtered to remove laser scatter. The measured fluorescence is directly correlated to NO_2 following calibration to a NIST traceable NO_2 calibration standard (accuracy of ±5 %). The NO_2 calibration constant was determined and applied as a function of inlet pressure due to the non-linear response of the system to pressure, a result of reduced jet-cooling of NO_2 at low ambient pressures. Higher order reactive nitrogen classes (ΣPNs, ΣANs and HNO_3) are detected by coupling a thermal dissociation inlet to the LIF sensor (Day et al., 2002). In this system, we heat the ambient air stream to the dissociation threshold for the class of NO_y species of interest (200 °C for ΣPNs, 350 °C for ΣPNs + ΣANs, and 550 °C for ΣPNs + ΣANs + HNO_3) and detect the NO_2 dissociation product using NO_2 LIF. As configured for INTEX-B N_2O_5 and $ClNO_2$ if present would be detected in the ΣPNs channel. The resulting system has an NO_2 detection limit of 8 pptv/10 s at 760 Torr (ground) and 25 pptv/10 s at 10 km at $S/N = 2$. The sensitivity of the TD-LIF technique toward ΣPNs, ΣANs and HNO_3 is determined by the partitioning of the individual components of NO_y as discussed in Day et al. (2002).

3 Results

3.1 Observations of reactive nitrogen during INTEX-B

The vertical distribution in the sum of the measured gas-phase components of NO_y (here defined as NO_x + ΣPNs + ΣANs + HNO_3) are shown in Fig. 2, alongside the vertical profile in ozone for observations made both North (Fig. 2a) and South (Fig. 2b) of 35° N. Observations were separated into 1 km altitude bins, where the median in each bin is shown with a solid line, and the shaded region represents the interquartile range of the observations. The fraction of NO_y carried by particulate NO_3^- is not shown in Fig. 2, due to sparse data coverage, and limited sampling during vertical profiling. The contribution of particulate NO_3^-, as measured using mist chamber – ion chromatography (Talbot et al., 1997), to the NO_y budget is shown in Fig. 3, and discussed below. The observed range in gas-phase NO_y mixing ratio (200–400 pptv) is broadly consistent with the small set of previous observations of NO_y in the Pacific. Further, the vertical distribution of O_3 and NO_y are correlated in the troposphere reflecting their coupled source and sink mechanisms.

The partitioning of NO_y, between NO_x, ΣPNs, ΣANs, HNO_3, and aerosol nitrate is shown in Fig. 3 as a function of altitude. Here, the fraction of NO_y in each altitude bin was calculated from the mean profile in each of the individual constituents. In the upper troposphere (above 10 km), NO_y is largely composed of HNO_3, due to transport of stratospheric air, rich in HNO_3, to the upper troposphere and the occasional sampling of purely stratospheric air in the Northern Pacific where the tropopause height (less than 10 km) is lower than the DC-8 aircraft ceiling (12.5 km). In the mid troposphere (4–10 km) ΣPNs comprise as much as 80 % of total NO_y. The dominance of ΣPNs in the NO_y budget is expected in the mid-troposphere due to their extended lifetime with respect to chemical, photolytic and heterogeneous removal processes (Talukdar et al., 1995) and the presence of sufficient VOC precursors of the peroxy acetyl radical. In the lower troposphere (below 4 km), the ΣPN fraction again decreases. This is a result of the strong temperature dependence in the PAN thermal dissociation rate constant,

where the thermal lifetime of PAN (at 35° N) goes from 20 days at 6 km to approximately two days at 4 km (Fig. 4). As a result, PAN thermal dissociation represents a significant source of NO_x to the remote troposphere. However, the NO_x lifetime with respect to reaction with OH is short, thus NO_x produced by ΣPN decomposition is converted to HNO_3 on the time scale of days. The large fraction of HNO_3 in the lower troposphere is likely a result of the oxidation of NO_x, formed from the thermal dissociation of PAN in subsiding air-masses. However, we cannot rule out the possibility of direct HNO_3 transport from the Asian continent to the sampling region. In the presence of mineral dust aerosol, gas-phase HNO_3 readily reacts heterogeneously with $CaCO_3$ resulting in the sequestration of nitrate in the particle phase as shown in Fig. 3 (McNaughton et al., 2009).

3.2 Latitudinal gradients in ΣPNs

Latitudinal gradients in PAN have been observed previously in the lower troposphere (Singh et al., 1998; Heald et al., 2003; Hudman et al., 2004). This is due to the strong temperature dependence in the PAN thermal dissociation rate as shown in Fig. 4. At 2 km altitude, the PAN lifetime to thermal dissociation increases from 12 h at 30° N to over 10 days at 50° N, at which point photolysis becomes the dominant loss process. The effect of PAN thermal dissociation is shown clearly in the vertical distribution of NO_y partitioning as a function of latitude. As shown in Fig. 3, ΣPNs comprise over 40 % of NO_y from the surface to the tropopause north of 35° N. In contrast, southern samples (latitudes below 35° N) show a strong shift from the NO_y budget being controlled by ΣPNs to being dominated by the sum of HNO_3 and particulate NO_3^- at low altitudes, consistent with the profile shape of the PAN thermal dissociation rate.

4 Discussion

4.1 Implications of Rising NO_y on Ozone Production Rates

The production rate of O_3 in the troposphere is primarily controlled by the cycling of NO_x in the presence of volatile organic carbon (VOC), oxidants and sunlight. In order to accurately model current O_3 abundances and assess the impact of future control strategies, it is critical to attain a mechanistic understanding of the chemical processes that drive O_3 production in the troposphere.

Since the steady-state relationship of NO and NO_2 directly impacts both O_3 concentrations and our interpretation of the production and loss mechanisms that control its abundance, it is useful to think separately about the abundances of odd oxygen, $O_x \equiv O_3 + NO_2 + O(^3P) + O(^1D)$, and to partition O_x according to the steady-state relationships. To investigate the dependence of O_x production on NO_x, we calculate the instantaneous net O_x production rate (ΔO_x) directly from measurements of NO (chemiluminescence), NO_2 (LIF; Thornton et al., 2000), OH and HO_2 (LIF; Faloona et al., 2004), H_2O (Diode laser hygrometer; Diskin et al., 2002), and O_3 (chemiluminescence; Fairlie et al., 2007), and calculations of $O(^1D)$ and RO_2 made using a photochemical box model constrained by observations of C1-C5 straight chain hydrocarbons, acetone, acetaldehyde, and peroxynitrates using Eqs. 6–8 (Thornton et al., 2002).

$$\Delta_{O_x} = P_{O_x} - L_{O_x} \tag{6}$$

$$P_{O_x} = k_{NO+HO_2}[NO][HO_2] + \sum_i k_{NO+RO_2(i)}[NO][RO_2(i)] \tag{7}$$

$$L_{O_x} = k_{OH+NO_2+M}[M][NO_2][OH] + k_{O(^1D)+H_2O}[O(^1D)][H_2O] + k_{HO_2+O_3}[O_3][HO_2] + k_{OH+O_3}[O_3][OH] \tag{8}$$

The dependence of ΔO_x on NO_x is shown in Fig. 5a, where ΔO_x is calculated from atmospheric measurements of the components defined in Eqs. (6)–(8), for all INTEX-B samples where the PAN lifetime was less than ten days. The frequency distribution of

NO_x mixing ratio is shown in Fig. 5b. While this analysis averages over a wide variety of chemical environments and VOC reactivity, it is instructive in describing the mean behavior of the lower troposphere over the remote pacific and its sensitivity to increasing NO_x loadings.

As shown in Fig. 5a, ΔO_x increases linearly with increasing NO_x, exhibiting NO_x-limited behavior over the entire sampling regime. In this low NO_x regime, the crossover point between net O_x destruction and net O_x production, has been identified at around 60 pptv, consistent with the early work of Fishman et al. (1979). This key diagnostic is critical for assessing how future increases in NO_x emissions will affect global O_3 abundances and illustrates the extreme sensitivity of the global O_3 budget to increasing NO_x. As a result, quantifying the magnitude and spatio-temporal distribution of NO_x and its transport and chemical evolution is crucial for modeling of tropospheric O_3.

4.2 Intercontinental transport of reactive nitrogen

The extent to which the rapid increases in NO_x emissions, observed over East Asia during the past decade (Richter et al., 2005; Q. Zhang et al., 2007), impact ozone production rates in the remote North Pacific and set the western boundary condition for North American regional air quality models is dependent on the chemical transformations that occur post emission and the export efficiency of NO_y from the source region to the free troposphere. NO_x emissions estimates over East Asia have been calculated using both top-down (Richter et al., 2005; L. Zhang et al., 2008; Walker et al., 2010) and bottom-up (Streets et al., 2003; Q. Zhang et al., 2009) techniques. Due to rapid increases in NO_x emissions, we compare our observations with emission inventories that were calculated for the 2006 INTEX-B sampling period. Specifically, Zhang et al. (2009) estimated the total East Asian anthropogenic emissions of NO_x to be 36.7 $Tg\,NO_x\,yr^{-1}$ for 2006, where 20.8 $Tg\,NO_x\,yr^{-1}$ were attributed to anthropogenic emissions in China. Using a top-down approach, L. Zhang et al. (2008) calculated that the 2000 TRACE-P East Asian anthropogenic NO_x emissions inventory of Streets

et al. (2003) (6.9 $Tg\,N\,yr^{-1}$) needed to be increased by a factor of two to match 2006 OMI NO_2 observations.

The fraction of reactive nitrogen emissions that leave the boundary layer is dependent on both the transport mechanism and the partitioning of reactive nitrogen between its soluble and insoluble forms. Measurements made during the TRACE-P field campaign in 2000 indicated that the time averaged export flux of NO_y across the 130° E meridonial plane between 30° and 40° N was 8 % between 0 and 2 km and 10 % between 2 and 7 km (Koike et al., 2007). The measurements of Koike et al. indicate that a total of 18 % of emitted NO_y is transported out of the source region. Using a similar analysis applied to the East Coast of the US, Li et al. (2004) determined that 17 % of NO_x emissions were exported out of boundary layer.

During INTEX-B, the DC-8 sampled between 25° and 55° N in the region of 135°–165° W (Fig. 1a). This sampling domain is characterized by zonal flow from Asia to North America with higher wind speeds recorded at higher altitudes and in the Northern section of the sampling domain (Hudman et al., 2004). To calculate the flux of nitrogen across the North Pacific between 25° and 55° N, we first construct curtain plots from the mean values of the observed wind speed and gas-phase NO_y number density binned into 2 km altitude and 5° latitude bins. We then calculate the flux as the product of these two observable properties (Fig. 6). The total daytime flux through this window for the INTEX-B sampling period is $0.007 \pm 0.002\,Tg\,N\,day^{-1}$. The observed gas-phase NO_y flux is 10 % NO_x, 62 % total peroxyacyl nitrates, 5 % alkyl nitrates and approximately 23 % nitric acid. Particulate nitrate was not included in the above analysis due to sparse data coverage. Based on trajectory analysis, it is expected that the majority of Asian emissions lofted to the free troposphere pass through this sampling window. As a result, the calculated flux can be used as an upper limit to the product of the emission rate and export efficiency, as the observed NO_y is also impacted by other sources such as Siberian biomass burning and stratospheric exchange. Using the Zhang et al. bottom up inventory for East Asia (17.12 $Tg\,N\,yr^{-1}$), our observation represents an upper limit of 15 % for the export of NO_y to the free troposphere.

4.3 NO_x production rates

To investigate the chemical and thermal repartitioning of NO_y in the INTEX-B sampling region, we calculate the diurnally averaged, altitude dependent NO_x production rates (molecules cm^{-3} s^{-1}) from the thermal decomposition of ΣPNs and the photolysis and reaction of hydroxyl radicals with HNO_3 using our ambient observations coupled with the aforementioned time-dependent chemical box-model. As shown in Fig. 7, the fraction of NO_x produced from ΣPNs is strongly altitude dependent, reflecting both the temperature dependence in the thermal decomposition rate and the concentration profile shown in Fig. 4. As a result, NO_x production from HNO_3 becomes an increasing fraction of the total production rate with increasing altitude, accounting for nearly 30 % of in situ NO_x production above 5 km. This further highlights the importance of accurate representation of HNO_3 in chemical transport models.

4.4 Role of episodic subsidence events in O_3 production

As discussed in Sect. 4.1, and shown in Eqs. 6–8, the net production rate of O_3 is not only dependent on the NO_x mixing ratio, but can be significantly impacted by the scavenging of $O(^1D)$ radicals by H_2O. As a result, we expect the most rapid net ozone production rates to be found in dry subsidence events where NO_x concentrations are high and water vapor mixing ratios low. In Fig. 8, the vertical profile in atmospheric water vapor is shown colored by ozone (top), ΣPNs (middle) and net ozone production rate (bottom) as calculated using a time-dependent box-model. The observations were filtered to remove strong stratospheric influence ($O_3/CO > 1.25$) and are for the Northern Pacific sampling domain (Latitude > 35° N). For comparison, the black hatched region in each panel corresponds to the range of conditions captured by the GEOS-CHEM model, sampled concurrently along the DC-8 flight track.

Both the calculated net ozone production rate, and the observed ozone mixing ratio indicate that rapid net ozone production (as high as 5×10^5 molecules cm^{-3} s^{-1}) can occur at low water vapor mixing ratios, resulting in ozone concentrations that are on

average 19.4 ppb higher that the corresponding mean value at higher water vapor mixing ratios (e.g. mean $O_3 = 73.2 \pm 14.4$ for measurements outside of the model domain, as compared to 53.8 ± 12.2 for those within the model water vapor domain). Below 6 km, 14.7 % of the observations were outside the model H_2O domain. This analysis suggests that episodic dry subsidence events that are characterized by high net ozone production rates, a result of suppressed quenching of $O(^1D)$ at low water vapor mixing ratios, likely play an important role in the intercontinental transport of ozone and its precursors from East Asia to North America. Specifically, these observations suggest that accurate representation of low water vapor mixing ratios within subsiding plumes is required to replicate calculations of $\Delta(O_3)$ as high as 5×10^5 molecules cm^{-3} s^{-1}.

5 Conclusions

The observations presented here provide experimental measures of the partitioning of reactive nitrogen in the remote Pacific and provide a novel opportunity to test model representations of the transport and chemical evolution of NO_y from the Asian continent. In agreement with previous studies, we find a dominant role for ΣPNs throughout the Pacific region, displaying a strong latitudinal dependence, consistent with the known temperature dependence in the thermal dissociation of PAN. The observations presented here reveal the extreme sensitivity of the remote North Pacific to future changes in NO_x loadings. Using simultaneous observations of speciated gas-phase NO_y and wind speed we calculate the net flux of reactive nitrogen through the meridional plane of 150° W to be 0.007 ± 0.002 Tg N day^{-1}, providing an upper limit of 15 % on the export efficiency of NO_y from East Asia. Box-model calculations, constrained by in situ observations, indicate that net ozone production is rapid in dry subsidence events where NO_x concentrations are high and water vapor mixing ratios low, indicating that chemical transport models attempting to predict enhancements in net ozone production rates need to simultaneously predict increases in NO_x as well as decreases in H_2O mixing ratios in subsidence events.

Appendix A

Stratospheric influence

The observations presented here were first filtered to remove strong stratospheric influence ($O_3/CO > 1.25$). Figure A1 shows a correlation plot of water vapor and CO illustrating the choice of the $O_3/CO = 1.25$ threshold for distinguishing samples that have strong stratospheric origin.

Acknowledgements. The authors thank the flight and ground crews of the NASA DC-8 Aircraft and the entire INTEX-B science team for their contributions during the 2006 intensive field campaign. We acknowledge Glen Sachse, Glenn Diskin, Greg Huey, Bill Brune, Jim Crawford, and Daniel Jacob for contributed data and/or model results. Work at U.C. Berkeley was supported under NASA grants NNX08AE56G, NNG05GH196, and NAG5-13668. The INTEX-B field program was supported by the NASA-ESE Tropospheric Chemistry Program. AEP acknowledges the NASA ESSF Program.

References

Arora, O. P., Cziczo, D. J., Morgan, A. M., Abbott, J. P. D., and Niedziela, R. F.: Uptake of nitric acid by sub-micron-sized ice particles, Geophys. Res. Lett., 26, 3621–3624, 1999.

Bertram, T. H. and Thornton, J. A.: Toward a general parameterization of N_2O_5 reactivity on aqueous particles: the competing effects of particle liquid water, nitrate and chloride, Atmos. Chem. Phys., 9, 8351–8363, doi:10.5194/acp-9-8351-2009, 2009.

Buhr, M. P., Parrish, D. D., Norton, R. B., Fehsenfeld, F. C., Sievers, R. E., and Roberts, J. M.: Contribution of organic nitrates to the total reactive nitrogen budget at a rural Eastern United-States site, J. Geophys. Res., 95, 9809–9816, 1990.

Calvert, J. G. and Madronich, S.: Theoretical-study of the initial products of the atmospheric oxidation of hydrocarbons, J. Geophys. Res.-Atmos., 92, 2211–2220, 1987.

Choi, W. and Leu, M. T.: Nitric acid uptake and decomposition on black carbon (soot) surfaces: its implications for the upper troposphere and lower stratosphere, J. Phys. Chem. A, 102, 7618–7630, 1998.

Day, D. A., Wooldridge, P. J., Dillon, M. B., Thornton, J. A., and Cohen, R. C.: A thermal dissociation laser-induced fluorescence instrument for in situ detection of NO_2, peroxy nitrates, alkyl nitrates, and HNO_3, J. Geophys. Res., 107, 4501, doi:10.1029/2003jd003685, 2002.

Day, D. A., Dillon, M. B., Wooldridge, P. J., Thornton, J. A., Rosen, R. S., Wood, E. C., and Cohen, R. C.: On alkyl nitrates, O_3, and the "missing NO_y", J. Geophys. Res., 108, 4046, doi:10.1029/2001jd000779, 2003.

Diskin, G. S., Podolske, J., Sachse, G., and Slate, T.: Open-path airborne tunable diode laser hygrometer, Proc. SPIE, 4817, 196–465, 2002.

Fairlie, T. D., Avery, M. A., Pierce, R. B., Al-Saadi, J., Dibb, J., and Sachse, G.: Impact of multiscale dynamical processes and mixing on the chemical composition of the upper troposphere and lower stratosphere during the intercontinental chemical transport experiment-North America, J. Geophys. Res.-Atmos., 112, D16S90, doi:10.1029/2006jd007923, 2007.

Faloona, I. C., Tan, D., Lesher, R. L., Hazen, N. L., Frame, C. L., Simpas, J. B., Harder, H., Martinez, M., Di Carlo, P., Ren, X. R., and Brune, W. H.: A laser-induced fluorescence instrument for detecting tropospheric OH and HO_2: characteristics and calibration, J. Atmos. Chem., 47, 139–167, 2004.

Farmer, D. K., Wooldridge, P. J., and Cohen, R. C.: Application of thermal-dissociation laser induced fluorescence (TD-LIF) to measurement of HNO_3, Σ alkyl nitrates, Σ peroxy nitrates, and NO_2 fluxes using eddy covariance, Atmos. Chem. Phys., 6, 3471–3486, doi:10.5194/acp-6-3471-2006, 2006.

Finlayson-Pitts, B. J., Wingen, L. M., Sumner, A. L., Syomin, D., and Ramazan, K. A.: The heterogeneous hydrolysis of NO_2 in laboratory systems and in outdoor and indoor atmospheres: an integrated mechanism, Phys. Chem. Chem. Phys., 5, 223–242, 2003.

Fishman, J., Solomon, S., and Crutzen, P. J.: Observational and theoretical evidence in support of a significant insitu photo-chemical source of tropospheric ozone, Tellus, 31, 432–446, 1979.

Heald, C. L., Jacob, D. J., Fiore, A. M., Emmons, L. K., Gille, J. C., Deeter, M. N.Warner, J., Edwards, D. P., Crawford, J. H., Hamlin, A. J., Sachse, G. W., Browell, E. V., Avery, M. A., Vay, S. A., Westberg, D. J., Blake, D. R., Singh, H. B., Sandholm, S. T., Talbot, R. W., and Fuelberg, H. E.: Asian outflow and trans-Pacific transport of carbon monoxide and ozone pollution: an integrated satellite, aircraft, and model perspective, J. Geophys. Res., 108, 4804, doi:10.1029/2003jd003507, 2003.

Hoell, J. M., Davis, D. D., Liu, S. C., Newell, R. E., Akimoto, H., McNeal, R. J., and Bendura, R. J.: The Pacific exploratory mission west phase B: February–March, 1994, J. Geophys. Res., 102, 28223–28239, 1997.

Hoell, J. M., Davis, D., Liu, S. C., Newell, R., Shipham, M., Akimoto, H., McNeal, R. J., Bendura, R. J., and Drewry, J. W.: Pacific exploratory mission-west A (PEM-West A): September October 1991, J. Geophys. Res., 101, 1641–1653, 1996.

Horowitz, L. W. and Jacob, D. J.: Global impact of fossil fuel combustion on atmospheric NO_x, J. Geophys. Res.-Atmos., 104, 23823–23840, 1999.

Hsu, N. C., Li, C., Krotkov, N. A., Liang, Q., Yang, K., and Tsay, S. C.: Rapid transpacific transport in autumn observed by the A-train satellites, J. Geophys. Res.-Atmos., 117, D06312, doi:10.1029/2011jd016626, 2012.

Hudman, R. C., Jacob, D. J., Cooper, O. R., Evans, M. J., Heald, C. L., Park, R. J., Fehsenfeld, F., Flocke, F., Holloway, J., Hubler, G., Kita, K., Koike, M., Kondo, Y., Neuman, A., Nowak, J., Oltmans, S., Parrish, D., Roberts, J. M., and Ryerson, T.: Ozone production in transpacific Asian pollution plumes and implications for ozone air quality in California, J. Geophys. Res., 109, D23S10, doi:10.1029/2004jd004974, 2004.

Jacob, D. J., Crawford, J. H., Kleb, M. M., Connors, V. S., Bendura, R. J., Raper, J. L., Sachse, G. W., Gille, J. C., Emmons, L., and Heald, C. L.: Transport and chemical evolution over the Pacific (TRACE-P) aircraft mission: design, execution, and first results, J. Geophys. Res., 108, 1–19, 2003.

Kirchner, W., Welter, F., Bongartz, A., Kames, J., Schweighoefer, S., and Schurath, U.: Trace gas-exchange at the air-water-interface – measurements of mass accommodation coefficients, J. Atmos. Chem., 10, 427–449, 1990.

Koike, M., Kondo, Y., Kita, K., Takegawa, N., Nishi, N., Kashihara, T., Kawakami, S., Kudoh, S., Blake, D., Shirai, T., Liley, B., Ko, M., Miyazaki, Y., Kawasaki, Z., and Ogawa, T.: Measurements of reactive nitrogen produced by tropical thunderstorms during BIBLE-C, J. Geophys. Res.-Atmos., 112, D18304, doi:10.1029/2006jd008193, 2007.

Lamarque, J. F., Brasseur, G. P., and Hess, P. G.: Three-dimensional study of the relative contributions of the different nitrogen sources in the troposphere, J. Geophys. Res.-Atmos., 101, 22955–22968, 1996.

Li, Q. B., Jacob, D. J., Munger, J. W., Yantosca, R. M., and Parrish, D. D.: Export of NO_y from the North American boundary layer: reconciling aircraft observations and global model budgets, J. Geophys. Res., 109, D02313, doi:10.1029/2003jd004086, 2004.

McNaughton, C. S., Clarke, A. D., Kapustin, V., Shinozuka, Y., Howell, S. G., Anderson, B. E., Winstead, E., Dibb, J., Scheuer, E., Cohen, R. C., Wooldridge, P., Perring, A., Huey, L. G., Kim, S., Jimenez, J. L., Dunlea, E. J., DeCarlo, P. F., Wennberg, P. O., Crounse, J. D., Weinheimer, A. J., and Flocke, F.: Observations of heterogeneous reactions between Asian pollution and mineral dust over the Eastern North Pacific during INTEX-B, Atmos. Chem. Phys., 9, 8283–8308, doi:10.5194/acp-9-8283-2009, 2009.

Moxim, W. J., Levy, H., and Kasibhatla, P. S.: Simulated global tropospheric PAN: its transport and impact on NO_x, J. Geophys. Res.-Atmos., 101, 12621–12638, 1996.

Munger, J. W., Wofsy, S. C., Bakwin, P. S., Fan, S. M., Goulden, M. L., Daube, B. C., Goldstein, A. H., Moore, K. E., and Fitzjarrald, D. R.: Atmospheric deposition of reactive nitrogen oxides and ozone in a temperate deciduous forest and a subarctic woodland, 1. Measurements and mechanisms, J. Geophys. Res.-Atmos., 101, 12639–12657, 1996.

Munger, J. W., Fan, S. M., Bakwin, P. S., Goulden, M. L., Goldstein, A. H., Colman, A. S., and Wofsy, S. C.: Regional budgets for nitrogen oxides from continental sources: variations of rates for oxidation and deposition with season and distance from source regions, J. Geophys. Res.-Atmos., 103, 8355–8368, 1998.

Noxon, J. F., Norton, R. B., and Henderson, W. R.: Observation of Atmospheric NO_3, Geophys. Res. Lett., 5, 675–678, 1978.

Parrish, D. D., Kondo, Y., Cooper, O. R., Brock, C. A., Jaffe, D. A., Trainer, M., Ogawa, T., Hubler, G., and Fehsenfeld, F. C.: Intercontinental transport and chemical transformation 2002 (ITCT 2K2) and Pacific exploration of Asian continental emission (PEACE) experiments: an overview of the 2002 winter and spring intensives, J. Geophys. Res., 109, D23s01, doi:10.1029/2004jd004980, 2004a.

Parrish, D. D., Ryerson, T. B., Holloway, J. S., Neuman, J. A., Roberts, J. M., Williams, J., Stroud, C. A., Frost, G. J., Trainer, M., Hubler, G., Fehsenfeld, F. C., Flocke, F., and Weinheimer, A. J.: Fraction and composition of NO_y transported in air masses lofted from the North American continental boundary layer, J. Geophys. Res., 109, D09302, doi:10.1029/2003jd004226, 2004b.

Platt, U., Perner, D., Winer, A. M., Harris, G. W., and Pitts, J. N.: Detection of NO_3 in the polluted troposphere by differential optical-absorption, Geophys. Res. Lett., 7, 89–92, 1980.

Richter, A., Burrows, J. P., Nuss, H., Granier, C., and Niemeier, U.: Increase in tropospheric nitrogen dioxide over China observed from space, Nature, 437, 129–132, 2005.

Sander, R.: Compilation of Henry's Law Constants for Inorganic and Organic Species of Potential Importance in Environmental Chemistry (Version 3) Rep., Mainz, Germany, 1999.
Shepson, P. B., Anlauf, K. G., Bottenheim, J. W., Wiebe, H. A., Gao, N., Muthuramu, K., and Mackay, G. I.: Alkyl nitrates and their contribution to reactive nitrogen at a rural site in Ontario, Atmos. Environ. A-Gen., 27, 749–757, 1993.
Singh, H. B., Salas, L. J., Ridley, B. A., Shetter, J. D., Donahue, N. M., Fehsenfeld, F. C., Fahey, D. W., Parrish, D. D., Williams, E. J., Liu, S. C., Hubler, G., and Murphy, P. C.: Relationship between peroxyacetyl nitrate and nitrogen-oxides in the clean troposphere, Nature, 318, 347–349, 1985.
Singh, H. B., Salas, L. J., and Viezee, W.: Global distribution of peroxyacetyl nitrate, Nature, 321, 588–591, 1986.
Singh, H. B., Salas, L. J., and Viezee, W.: Latitudinal distribution of reactive nitrogen in the free troposphere over the Pacific Ocean in late winter early spring, J. Geophys. Res., 103, 28237–28246, 1998.
Streets, D. G., Bond, T. C., Carmichael, G. R., Fernandes, S. D., Fu, Q., He, D., Klimont, Z., Nelson, S. M., Tsai, N. Y., Wang, M. Q., Woo, J. H., and Yarber, K. F.: An inventory of gaseous and primary aerosol emissions in Asia in the year 2000, J. Geophys. Res.-Atmos., 108, 8809, doi:10.1029/2002jd003093, 2003.
Talbot, R. W., Dibb, J. E., Lefer, B. L., Scheuer, E. M., Bradshaw, J. D., Sandholm, S. T., Smyth, S., Blake, D. R., Blake, N. J., Sachse, G. W., Collins, J. E., and Gregory, G. L.: Large-scale distributions of tropospheric nitric, formic, and acetic acids over the Western Pacific basin during wintertime, J. Geophys. Res.-Atmos., 102, 28303–28313, 1997.
Talukdar, R. K., Burkholder, J. B., Schmoltner, A. M., Roberts, J. M., Wilson, R. R., and Ravishankara, A. R.: Investigation of the loss processes for peroxyacetyl nitrate in the atmosphere – UV photolysis and reaction with OH, J. Geophys. Res.-Atmos., 100, 14163–14173, 1995.
Thornton, J. A., Wooldridge, P. J., and Cohen, R. C.: Atmospheric NO_2: in situ laser-induced fluorescence detection at parts per trillion mixing ratios, Anal. Chem., 72, 528–539, 2000.
Thornton, J. A., Wooldridge, P. J., Cohen, R. C., Martinez, M., Harder, H., Brune, W. H., Williams, E. J., Roberts, J. M., Fehsenfeld, F. C., Hall, S. R., Shetter, R. E., Wert, B. P., and Fried, A.: Ozone production rates as a function of NO_x abundances and HO_x production rates in the Nashville urban plume, J. Geophys. Res., 107, 4146, doi:10.1029/2001jd000932, 2002.

Tolocka, M. P., Saul, T. D., and Johnston, M. V.: Determination of nitric acid uptake onto sodium chloride particles, Abstr. Pap. Am. Chem. S., 224, U347–U347, 2002.
Trainer, M., Buhr, M. P., Curran, C. M., Fehsenfeld, F. C., Hsie, E. Y., Liu, S. C., Norton, R. B., Parrish, D. D., Williams, E. J., Gandrud, B. W., Ridley, B. A., Shetter, J. D., Allwine, E. J., and Westberg, H. H.: Observations and modeling of the reactive nitrogen photochemistry at a rural site, J. Geophys. Res.-Atmos., 96, 3045–3063, 1991.
Turnipseed, A. A., Huey, L. G., Nemitz, E., Stickel, R., Higgs, J., Tanner, D. J., Slusher, D. L., Sparks, J. P., Flocke, F., and Guenther, A.: Eddy covariance fluxes of peroxyacetyl nitrates (PANs) and NO_y to a coniferous forest, J. Geophys. Res., 111, 3045–3063, 2006.
Walker, T. W., Martin, R. V., van Donkelaar, A., Leaitch, W. R., MacDonald, A. M., Anlauf, K. G., Cohen, R. C., Bertram, T. H., Huey, L. G., Avery, M. A., Weinheimer, A. J., Flocke, F. M., Tarasick, D. W., Thompson, A. M., Streets, D. G., and Liu, X.: Trans-Pacific transport of reactive nitrogen and ozone to Canada during spring, Atmos. Chem. Phys., 10, 8353–8372, doi:10.5194/acp-10-8353-2010, 2010.
Wolfe, G. M., Thornton, J. A., Yatavelli, R. L. N., McKay, M., Goldstein, A. H., LaFranchi, B., Min, K.-E., and Cohen, R. C.: Eddy covariance fluxes of acyl peroxy nitrates (PAN, PPN and MPAN) above a Ponderosa pine forest, Atmos. Chem. Phys., 9, 615–634, doi:10.5194/acp-9-615-2009, 2009.
Yienger, J. J., Galanter, M., Holloway, T. A., Phadnis, M. J., Guttikunda, S. K., Carmichael, G. R., Moxim, W. J., and Levy, H.: The episodic nature of air pollution transport from Asia to North America, J. Geophys. Res., 105, 26931–26945, 2000.
Zhang, L., Jacob, D. J., Boersma, K. F., Jaffe, D. A., Olson, J. R., Bowman, K. W., Worden, J. R., Thompson, A. M., Avery, M. A., Cohen, R. C., Dibb, J. E., Flock, F. M., Fuelberg, H. E., Huey, L. G., McMillan, W. W., Singh, H. B., and Weinheimer, A. J.: Transpacific transport of ozone pollution and the effect of recent Asian emission increases on air quality in North America: an integrated analysis using satellite, aircraft, ozonesonde, and surface observations, Atmos. Chem. Phys., 8, 6117–6136, doi:10.5194/acp-8-6117-2008, 2008.
Zhang, Q., Streets, D. G., He, K., Wang, Y., Richter, A., Burrows, J. P., Uno, I., Jang, C. J., Chen, D., Yao, Z., and Lei, Y.: NO_x emission trends for China, 1995–2004: the view from the ground and the view from space, J. Geophys. Res.-Atmos., 112, D22306, doi:10.1029/2007jd008684, 2007.
Zhang, Q., Streets, D. G., Carmichael, G. R., He, K. B., Huo, H., Kannari, A., Klimont, Z., Park, I. S., Reddy, S., Fu, J. S., Chen, D., Duan, L., Lei, Y., Wang, L. T., and Yao, Z. L.: Asian

emissions in 2006 for the NASA INTEX-B mission, Atmos. Chem. Phys., 9, 5131–5153, doi:10.5194/acp-9-5131-2009, 2009.

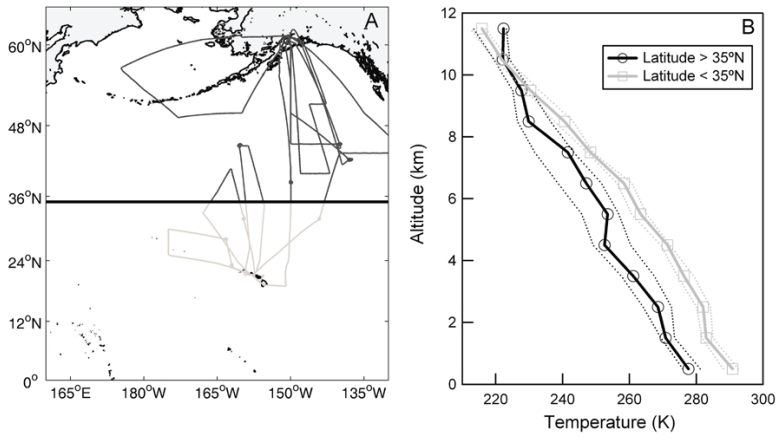

Fig. 1. Left panel: INTEX-B flight tracks made between 17 April 2006 and 15 May 2006 over the Northern Pacific Ocean. Sampling legs north of 35° N are shown in black, while legs south of 35° N are shown in grey. Right panel: observed mean temperature within 1 km altitude bins between 0–12 km divided into northern (black) and southern (grey) sampling bins. The dashed lines represent one standard deviation of the mean.

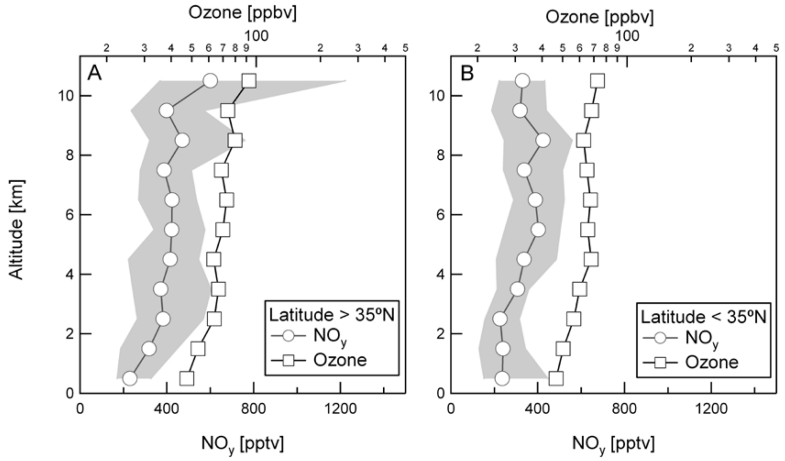

Fig. 2. Median vertical profile in ozone (black) and gas-phase NO_y (grey) ($NO_y \equiv NO_x + \Sigma PNs + \Sigma ANs + HNO_3$) as observed during the INTEX-B field campaign over the North Pacific during the spring of 2006 (April–May), north of 35° N left panel and south of 35° N right panel. The solid line depicts the median value in 1 km altitude bins and the shaded regions represent the interquartile range.

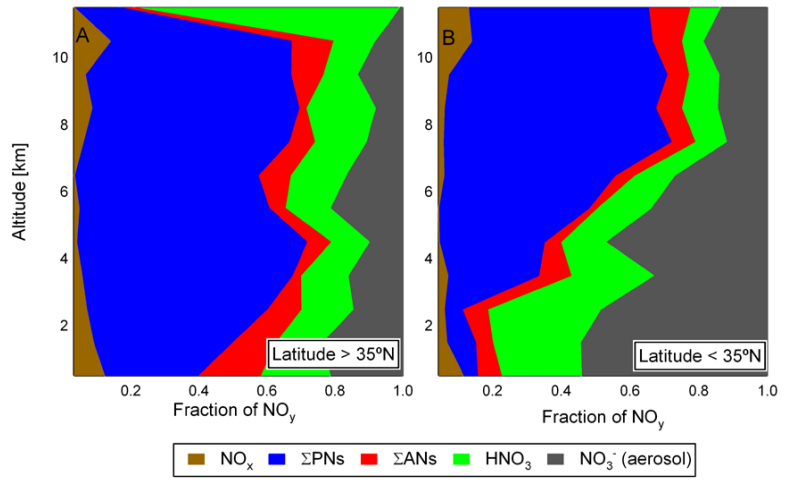

Fig. 3. Vertical distribution of the partitioning of reactive nitrogen (NO_y) between NO_x (brown), ΣPNs (blue), ΣANs (red), HNO_3 (green) and particulate nitrate (grey) as observed during the INTEX-B field campaign over the North Pacific during the spring of 2006 (April–May), north of 35° N (**A**) and south of 35° N (**B**). The fraction of NO_y in each altitude bin was calculated from the median profile in each of the individual constituents.

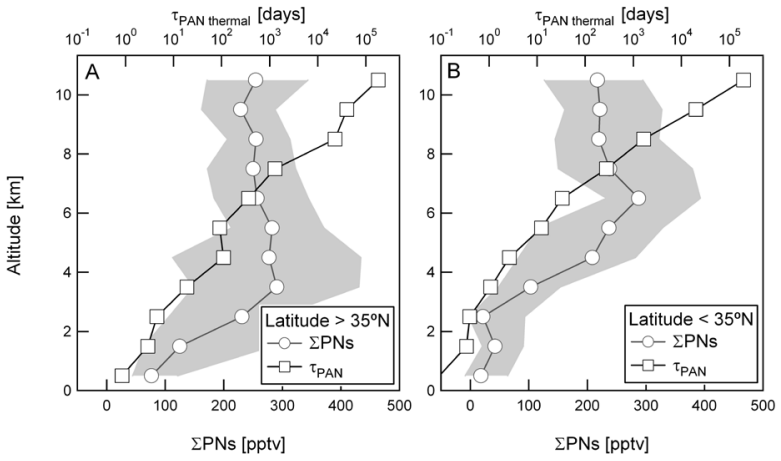

Fig. 4. Median vertical profile in ΣPNs (grey, -o-) and PAN thermal lifetime (τ_{PAN}) (black, -□-) as observed during the INTEX-B field campaign over the North Pacific during the spring of 2006 (April–May), north of 35° N (left panel) and south of 35° N (right panel). The solid line depicts the median value in 1 km altitude bins and the shaded regions represent the interquartile range.

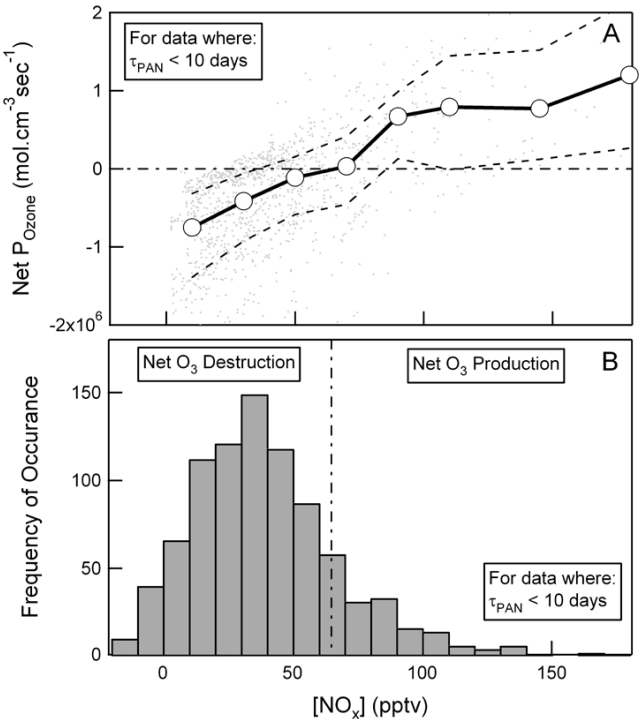

Fig. 5. Top panel: calculated instantaneous net ozone production rate as a function of NO_x. Bottom panel: observed frequency distribution of NO_x for air-masses where PAN lifetime (τ_{PAN}) is less than 10 days. Observations were filtered to strong remove stratospheric influence (O_3/CO > 1.25) and are for the Northern Pacific (Latitude > 35° N).

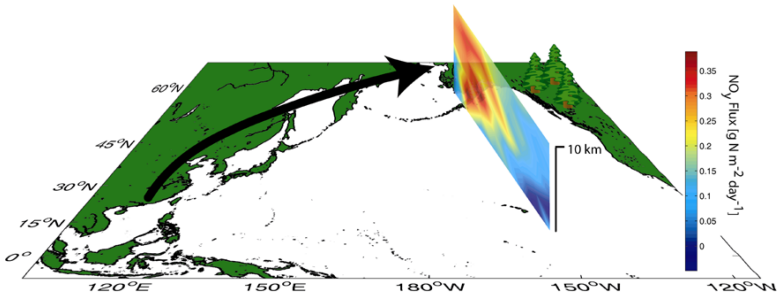

Fig. 6. Daytime flux of reactive nitrogen ($g N m^2 day^{-1}$) calculated using all available observations of gas-phase NO_y and wind-speed gridded into 5 latitude × 2 km altitude bins. Observations were filtered to strong remove stratospheric influence ($O_3/CO > 1.25$).

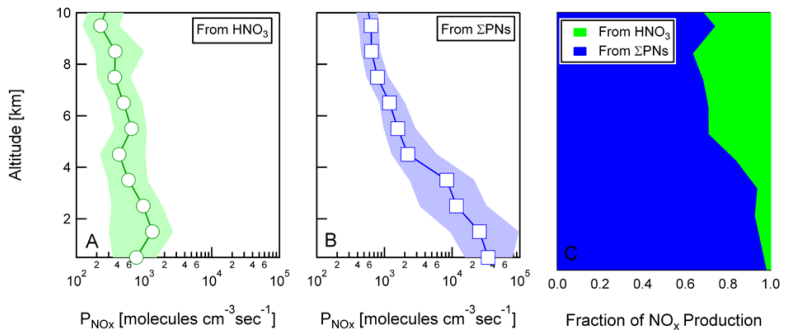

Fig. 7. Diurnally averaged NO_x production rates ($molecules\,cm^{-3}\,s^{-1}$) from nitric acid (left) and ΣPNs (center) as a function of altitude. The fraction of NO_x production from each channel is shown in the right panel. Observations were filtered to strong remove stratospheric influence ($O_3/CO > 1.25$) and are for the Northern Pacific (Latitude > 35° N).

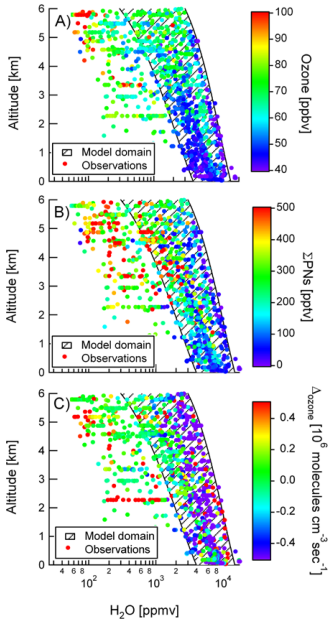

Fig. 8. Vertical profile in atmospheric water vapor, color coded by ozone (top), ΣPNs (middle) and net ozone production rate (bottom) as calculated using a time-dependent box-model. The black hatched region in each figure corresponds to mean conditions captured by chemical transport models. Observations were filtered to remove strong stratospheric influence (O_3/CO > 1.25) and are for the Northern Pacific (Latitude > 35° N).

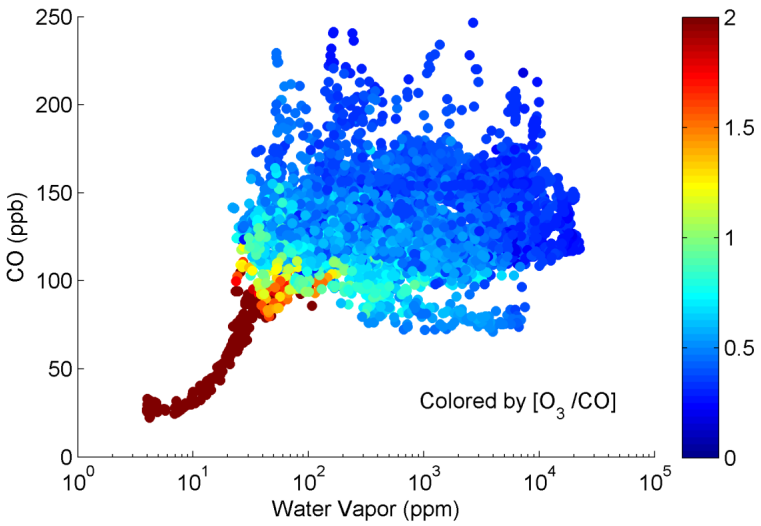

Fig. A1. Correlation plot of water vapor and carbon monoxide for the entire INTEX-B sampling domain. Observations that suggest strong stratospheric influence (O_3/CO > 1.25) were removed from the analysis.